Experimental Thermal and Fluid Science 65 (2015) 52–64

Contents lists available at ScienceDirect

Experimental Thermal and Fluid Science

journal homepage: www.elsevier.com/locate/etfs

An experimental investigation of the swirling flow in a tall-form counter current spray dryer

Victor Francia [a,b,*], Luis Martin [b], Andrew E. Bayly [b,1], Mark J.H. Simmons [a]

[a] School of Chemical Engineering, University of Birmingham, Birmingham, UK
[b] Procter & Gamble R&D, Newcastle Innovation Centre, Newcastle upon Tyne, UK

ARTICLE INFO

Article history:
Received 1 December 2014
Received in revised form 14 February 2015
Accepted 2 March 2015
Available online 7 March 2015

Keywords:
Spray drying
Vortex flow
Swirl decay
Friction
Downstream effects
PVC

ABSTRACT

This work studies the air flow in a large swirl counter-current dryer using sonic anemometry. Air velocity and turbulence fields are reported at isothermal conditions and in the absence of particles. In a tall-form unit the structure of the flow is largely influenced by the design of the exit. A contraction originates a central jet and suppresses the formation of recirculation zones despite the vortex acquires a high swirl intensity Ω (i.e. $1 < \Omega < 2$). Access to a full scale tower has permitted to: (a) identify asymmetries owed to the design of inlet and exhaust ducts, (b) present the first detailed turbulence data in production units, characterized by a highly anisotropic field and the axial decay of the turbulence kinetic energy, (c) study the flow stability, identifying the precession of the vortex core and oscillations at a constant Strouhal number and (d) study the impact that a rough wall has in the strength of the swirl. This work presents the first clear evidence of significant friction in spray dryers. The swirl intensity Ω decays exponentially in the dryer at a rate between 0.08 and 0.09, much higher than expected in pipe flow and independent of *Re* in the range 10^5–$2.2 \cdot 10^5$. Production dryers have a large characteristic wall roughness due the presence of deposits, which explains the stronger friction and the discrepancies found in the past between data at full scale or clean laboratory or pilot scale units. It is essential to address this phenomenon in current numerical models, which are validated on laboratory or pilot scale facilities and ignore the role of deposits, thus causing an overprediction of the tangential velocity above 30–40%.

1. Introduction

Among the main advantages of spray drying processes is the generation of low density granules with an open structure [1]. Product properties, particularly the morphology of the final granules, depend on the temperature history and the agglomeration undergone in the dryer, for which understanding the air fluid dynamics is a fundamental. Counter-current swirl dryers are used for the manufacture of thermally stable powders, such as detergents, and in occasions they apply strong swirling flows to enhance the heat and mass transfer and optimize the contact between the phases [2]. The structure of a strong turbulent swirling flow under confinement has been studied in detail for free developing or non-recirculating systems (i.e. also referred to as once through swirling flows, such as open pipes, tubes or concentric cylinders) and in systems where the confinement restricts the vortex development (i.e. combustors or cyclones). The study of large scale units such as a swirl drying tower is far more limited. In a long confinement the swirling motion decays due the development of the boundary layer and the action of the wall shear stress (frictional losses). This phenomenon is described in the research over open pipes (e.g. Kitoh [3]; Steenbergen and Voskamp [4]) and extended by Chang and Dhir [5,6] to a higher swirl intensity with the use of tangentially injected flows. By contrast, in a spray drying tower the swirl causes most of the solids to concentrate near the wall, and generates thick multi-layered deposits [7,8], which increase roughness and are expected to disrupt significantly the boundary layer and the structure of the turbulence [9,10].

Recirculation patterns and the stability in vortices are often studied in terms of the Reynolds number *Re* and the ratio between the angular and axial momentum, characterized by a swirl number or intensity, Ω. When the swirl develops in an open cylinder, at a sufficiently high intensity the adverse pressure gradient generated by the centrifugal force causes the reversion of the flow. This originates a central recirculation zone, denoted *CRZ*, in the region upstream. As the swirl decays along the cylinder, the centrifugal

* Corresponding author at: School of Chemical Engineering, University of Birmingham, Birmingham, UK.
E-mail address: v.francia.chemeng@gmail.com (V. Francia).
[1] Present address: School Chemical and Process Engineering, University of Leeds, Leeds, UK.

http://dx.doi.org/10.1016/j.expthermflusci.2015.03.004
0894-1777/

Nomenclature

A	swirl decay rate in Eq. (12)
A_c	cross sectional area in the cylinder, m^2
A_i	combined area of all inlet nozzles, m^2
B	swirl decay constant in Eq. (12)
D	diameter of the cylinder, m
G_θ	axial angular momentum flux, kg m^{-1} s^{-2}
G_z	axial momentum flux, kg s^{-2}
$\overline{M}_c$	mass rate through the cylinder, kg s^{-1}
$\overline{M}_i$	combined mass rate through the inlets, kg s^{-1}
H	distance from air inlets to vortex finder, m
P	static pressure, kg m^{-1} s^{-2}
R	radius of the cylinder, m
R_i	radius of the cross-section at the inlets, m
Re	Reynolds number $Re = DU_{av}/v$
S	swirl number in Eq. (6)
$\overline{U}$	time averaged air velocity, m s^{-1}
$\overline{U}_{av}$	bulk or superficial velocity, $\overline{U}_{av} = \overline{M}_c/\overline{\rho}A_C$, m s^{-1}
$\overline{U}_i$	velocity at the inlets, $\overline{U}_i = \overline{M}_i/\rho A_i$, m s^{-1}
St	Strouhal number, $St = f \cdot D/\overline{U}_{av}$
d	diameter of the vortex finder, m
f	oscillation frequency, Hz
r	coordinate in the radial direction, m
u	velocity fluctuation, m s^{-1}
x	distance from the centreline, m
z	axial position, m

Greek letters

Ω	swirl intensity
α	anemometer misalignment over a_2 in Fig. 2, rad
β	anemometer misalignment over a_3 in Fig. 2, rad
ε	roughness height, m
ξ	axial alignment of the air inlet nozzles, rad
γ	anemometer misalignment over a_1 in Fig. 2, rad
λ	swirl decay rate in Eq. (10).
κ	specific turbulent kinetic energy, m^2 s^2
ρ	density, kg m^{-3}
τ	shear stress, kg m^{-1} s^{-2}
υ	kinematic viscosity/Eddy viscosity, m^2 s^{-1}
φ	radial alignment of the air inlet nozzles, rad

Subscripts, superscripts

r, z, θ	along radial, vertical and tangential direction
$^\circ, -, +$	best estimate, under and over estimation
ref	a reference height, or length, in Eqs. (10) and (12).
w	at the wall

Abbreviations

CRZ	central recirculation region
PVC	precession of the vortex core
VBD	vortex breakdown

force decreases and a stagnation point forms, after which the flow reverses back in what is referred to as a vortex breakdown, *VBD*, that often carries some associated oscillations. The instabilities are complicated by the interaction with the design in cases where the confinement is more restrictive, such as in a combustor or a drying tower. In these units, an increase in Ω or Re interacts in a more complex manner with the exit boundaries, which is referred to as downstream effects. Escudier et al. [11], Escudier and Keller [12] or Derksen [13] provide a detailed study of the effect that an exit contraction can have in stabilizing the flow upstream. The origin of periodic oscillations associated to the *VBD*, such as the precession of the vortex core, *PVC*, has been discussed extensively in the case of combustors [14] and cyclonic flows [15,16]. While these are beneficial in combustion, for they increase mixing and stabilize the flame, they are considered detrimental to the collection efficiency in cyclones. In co-current dryers, the studies of turbulence of among others, Usui et al. [17], Langrish et al. [18] and Kieviet et al. [19] report similar aerodynamic instabilities, followed by the work of Southwell and Langrish [20] and Langrish et al. [21], but no data in this regard is available for counter-current swirl units.

It is also very important to provide turbulence data in swirl dryers because large numerical simulations often lack any means to evaluate how the closure models actually perform. In counter-current swirl units an accurate turbulence prediction is particularly important to (a) determine the elutriation of fines, which concerns with the description of a high angular velocity core [22] and requires the application of a Reynolds-Stress Transport Model, *RSTM* [23,24], (b) describe the flow near the wall, in particular, assess how semi-empirical functions for rough walls could apply to strong swirling flows [24], (c) obtain an adequate replication of anisotropy and particle dispersion, and (d) the description of the aerodynamic instabilities observed experimentally, which increase the level of mixing and affect the inner jet.

In spite of the complexities above, experimental data on the air flow patterns in counter-current tall form dryers are rare and very restricted in nature. The studies in pilot scale facilities included flow visualization and *RTD* analysis reported by Place et al. [25], Paris et al. [26] and Sharma [22] or Keey and Pham [27] in co-current units. Only in the last decade a higher level of detail has been obtained by taking advantage of laser-based flow diagnostic techniques in laboratory [28] or pilot plant units [29]. Data at production scales is much more restricted, from vane [30] to thermal anemometers [31], and a similar level of detail is not yet available. Detailed studies are of small scope and limited to particle image velocimetry, *PIV*, analysis near the wall [7].

This paper addresses the lack of data at a full scale providing the flow characterization on an industrial spray drying tower at isothermal conditions and in the absence of particles. Time average velocity and the turbulence field are reported at the cylindrical chamber of the unit. The common features to similar swirling flows in pipes, combustors or cyclones are discussed, including (a) the effects linked to the design of an exit contraction, Section 4.1.1, and Re, Section 4.1.2, (b) the asymmetry, Section 4.1.3, (c) the effect of wall roughness and the decay of the swirl intensity, Section 4.1.4, (d) the description of turbulence, Sections 4.2.1–4.2.3 and (e) periodic structures, Section 4.2.4.

2. Unit and instrumentation

An industrial scale counter-current swirl spray drying tower has been used for the conduction of the measurements, property of Procter & Gamble Co. The main design features are depicted in Fig. 1a, including the nomenclature and location of measurements. The air delivery system consists of inlet and exhaust fans, set manually to deliver a constant flow rate to the tower and a target exit pressure. Table 1 summarizes the design and the operating conditions. The air enters the unit near the bottom of the cylindrical body through a series of symmetrical nozzles, and exits through a top conduit, known as tubular guard or vortex finder. The alignment of the inlet ports, shown in Fig. 1b, imparts the flow with

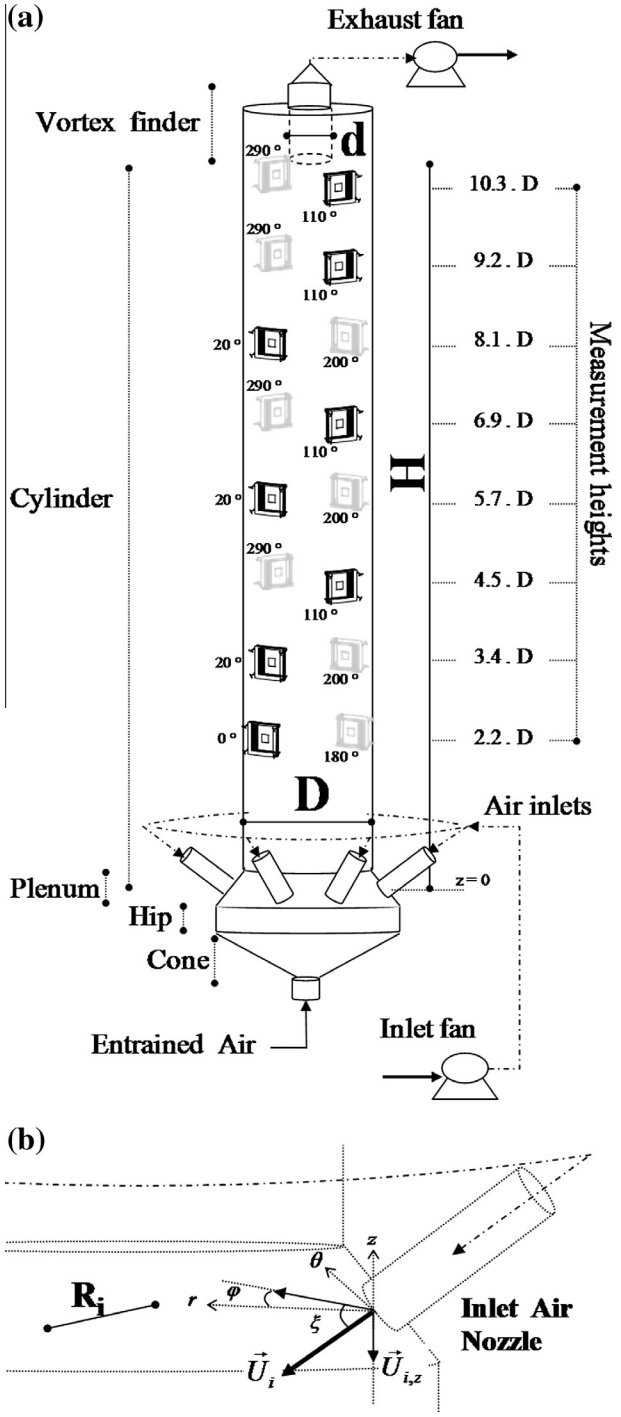

Fig. 1. (a) General outline of the sections of a counter-current spray drying tower, the air delivery system and the swirl generation mechanism. (b) Detail of the alignment of the air inlet nozzles/ports.

Table 1
Tower design parameters, and operating conditions. $\overline{U}_{av} = \overline{M}_C/\bar{\rho}A_C$ and Reynolds number $Re = \bar{\rho} \cdot D \cdot \overline{U}_{av}/\bar{\mu}$.

Design parameters		Operation $Re \cdot 10^{-5}$		$\overline{U}_{av}/\overline{U}_{av,Re_1}$
H/D	10.58	Re_1	1.06 ± 0.03	0.98–1.02
d/D	0.29	Re_2	1.49 ± 0.02	1.39–1.44
Ω_i	5.1–5.4	Re_3	2.22 ± 0.02	2.09–2.17

angular momentum, generating the swirl and the formation of a vortex in the conical section, which then rises into the cylinder

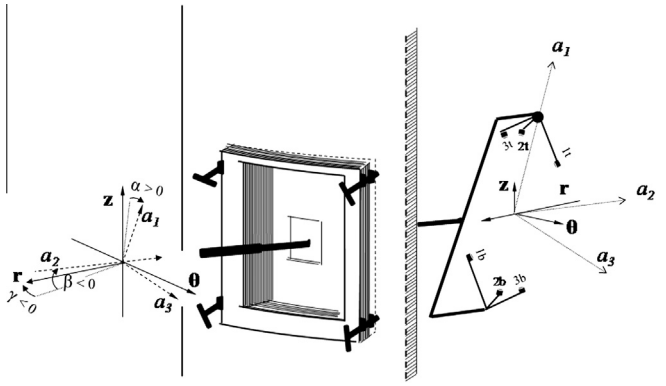

Fig. 2. Anemometer ensemble. The deviations between the door and the inner wall and the rotation of the head lead to a series of misalignments between the anemometer measurement axes, $a_1a_2a_3$ and the polar reference frame, $rz\theta$.

above. The alignment, φ and ξ to the radial and axial axes respectively determines the initial intensity of the swirl, Ω_i defined later as the non-dimensional flux of angular momentum normalized by the axial momentum based upon the superficial velocity $\overline{U}_{av}$. In isothermal conditions, it reads

$$\Omega_i = \frac{G_{\theta,i}}{R \cdot G_{z,av}} = \frac{\overline{M}_i \overline{U}_{i,\theta} R_i / \pi R^2}{\overline{M}_C \overline{U}_{av} R / \pi R^2} = \frac{\overline{M}_i^2}{\overline{M}_C^2} \frac{A_C}{A_i} \frac{R_i}{R} \cdot \sin\varphi \cos\xi \quad (1)$$

Ω_i is an exclusive function of the geometry and constitutes a characteristic design parameter, in the same manner that the geometric swirl number is a characteristic of cyclones [32]. It results from 1 – the inlets alignment, 2 – the ratio between the mass rates through the inlets $\overline{M}_i$ and the cylinder $\overline{M}_C$ (owed to entrainment of air from the bottom end) and 3 – the contraction ratios specific to the tower design, between the radius at the cylinder R_C and that at the inlet R_i ring, and the combined area of all inlets, A_i and that of the cylinder, A_C.

In the operation of counter-current towers the deposits grow considerably and distribute heterogeneously. This work however maintains homogeneous roughness with a twofold purpose: (a) replicate the best scenario in industry given by recently "cleaned" walls, and (b) ensure an easier numerical reproduction. Further experimental work [33] investigates the role of the deposits at the wall, comparing this reference to the flow field established under deposits of different thickness and coverage. In this case, reproducible conditions were obtained by cleaning the inner surface with an automatic ring designed to ensure the layer of deposits is thinner than 0.006D. A perfectly homogeneous layer cannot be obtained, but rather a coarse definition is given whereby the roughness height ε ranges between 0 and 0.006D.

A Horizontal Symmetry Sonic Solent Anemometer HS-50 (Gill Instruments Ltd.) [34] served to acquire velocity measurements, depicted in Fig. 2. Three independent pairs of ultrasonic transducers alternate to emit and receive an acoustic pulse >$4 \cdot 10^4$ Hz [35]. Analysis of the propagation velocity allows one to derive the velocity of the medium along three independent directions in a finite sampling volume and with a temporal resolution of 50 Hz. Measurements were gathered during 60 s (~3000 samples). The data may be considered a spatial average across the pulse path in a steady non-uniform field operating at very low Mach numbers [36]. The potential effect of averaging and the shift of the sonic pulse are minimized because the paths are almost vertical and axial gradients are very small, with the exception of the central region where the errors are higher, similarly to sensors of a finite size [3].

A door was engineered *adhoc* to assemble around the anemometer frame, as shown in Fig. 2. This allows the centre of the sonic path to be placed at any desired location in the tower by sliding the frame

inwards, along a_2, so that in all cases, the axis a_1 is kept aligned with the tower axial coordinate z, which is required to minimize all the sources of error and the gradients in the sonic paths. Wind tunnel calibrations valid <45 ms^{-1} establish the accuracy as <1% *RMS* in velocity magnitude and 1° in direction. However, the technique is reapplied here to confined spaces and one must address the question of how the local disturbance can affect the measurement or distortion the flow field. The uncertainty depends on the orientation the instrument versus the air flow direction, known as attack angle, and the turbulence [37]. Errors vary from one to another location because the HS-50 keeps a constant orientation but the flow varies. The maximum range of uncertainty was quantified in the range of attack angles and turbulence levels characteristic of this application, by orientating the HS-50 in all possible angles at various sections of a long confined vortex [38,39]. The method is less accurate than the use of anemometers in atmospheric studies, or the use of lasers, hot-wires [3] or thermal anemometers [40] but it is more flexible and cost effective, which permits conducting experiments in industrial units (volumes > 100 – 1000 m^3) where data is more limited [31]. In regions of the vortex that comply with the limit attack angles, errors are <1–4% in the velocity magnitude, <3° in direction and <7–31% in turbulent kinetic energy, κ. In others, such as the central region, the flow attacks the HS-50 from the bottom and a stronger disruption results in a large deficit bias in the velocity. Fig. 2 defines the frames of reference for the anemometer and the tower cylinder, and the various alignments used to determine the measurement position and the instrument orientation. Measurements were carried out in all the accesses shown in Fig. 1a to gather, 240 individual locations in the cylinder, at 8 vertical levels, 2 tangential coordinates and 15 radial positions for each *Re*. The velocity and turbulence profiles obtained are in agreement with the measurement of the volume rate in the dryer, past laser based methods [7] and recent improved models studying friction [24].

3. Analysis

3.1. Fluid dynamics parameters

At each location and *Re*, the time averaged velocity magnitude $\overline{U}$ and direction are obtained from a measurement at a sampling frequency of 50 Hz during 60 s. The Reynolds decomposition serves to compute the time series of instantaneous velocity fluctuations u_r, u_θ, u_z from which the stress tensor is obtained as normal $\overline{u_i u_i}$ and Reynolds stresses $\overline{u_i u_j}$ and the turbulent kinetic energy computed as $\kappa = 1/2(\overline{u_r u_r} + \overline{u_\theta u_\theta} + \overline{u_z u_z})$. Averaged profiles of the axial and tangential velocity components, $\overline{U}_z$ and $\overline{U}_\theta$ are available at a higher accuracy. Under the assumption of an axi-symmetrical system the azimuthal average of $\overline{U}_z$ and $\overline{U}_\theta$ permits one to estimate the average radial velocity profile $\overline{U}_r$, that satisfies the continuity equation below, where compressibility effects may be neglected.

$$\nabla \cdot (\rho U) = \frac{\partial \rho}{\partial t} \tag{2}$$

Velocity gradients are computed with the spatial grid generated and eddy viscosities are estimated with Eqs. (3)–(5) [3] assuming an axi-symmetrical system and away from the exit where $\partial \overline{U}_r / \partial z$ can be neglected.

$$v_{r,z} = -\frac{\overline{u_r u_z}}{\partial \overline{U}_r / \partial r} \tag{3}$$

$$v_{r,\theta} = -\frac{\overline{u_r u_\theta}}{r \cdot \partial\left(\frac{\overline{U}_\theta}{r}\right)/\partial r} \tag{4}$$

$$v_{z,\theta} = -\frac{\overline{u_z u_\theta}}{\partial \overline{U}_\theta / \partial z} \tag{5}$$

In addition to turbulence, the variability of velocity is also affected by the presence of periodical flow structures in the vortex. Their characteristic time scales are identified by applying a fast Fourier transform, *FFT*, to the velocity signal.

3.2. Swirl intensity

A circulation parameter, denoted swirl number or intensity, is often used to provide a general description of swirling flows. It defines at a cross section the ratio between the angular momentum flux, G_θ, to the axial momentum flux, G_z, given below (i.e. [41]):

$$S = \frac{G_\theta}{G_z \cdot R} \tag{6}$$

Strict integral definitions for G_θ and G_z derive from the conservation of momentum and angular momentum and require knowledge of static pressure and the turbulent terms [42]. Often they are too convoluted for many practical applications, which has generalized the use of simplified swirl numbers where momentum fluxes are estimated only on the basis of the convective flow, either excluding turbulence and/or static pressures, or estimating the latter through the tangential velocity profiles. In the unit investigated here the exit duct constitutes a 90% contraction of the flow area, which causes the acceleration of the flow and substantial changes in the pressure field. For that reason, an estimate of G_z neither accounting for the pressure term nor including accurate velocity measurements in the core region is not likely to be axially preserved, at least at the upper part of the cylinder, which would complicate the interpretation of S. The main focus of this work is not concerned with aerodynamic instabilities highly dependent on S, but rather examines the preservation of the swirl, which is especially relevant for the dynamics of the solid phase. On this basis, this work will follow the more usual practice in the study of decaying swirling flows in open cylinders by normalizing G_θ in (6) by a constant mean axial momentum flux $G_{z,av}$ [43]. The resulting swirl intensity, Ω, is then defined as the non-dimensional flux of angular momentum normalized by the axial momentum flux $G_{z,av}$ based on the superficial air velocity $\overline{U}_{av}$. This has been simplified to the expression below given by Kitoh [3].

$$\Omega = 2\pi\rho \int_0^R \frac{\overline{U}_z \overline{U}_\theta}{\rho \pi \overline{U}_{av}^2 R^3} r^2 \cdot dr \tag{7}$$

Other popular definitions, perhaps of a more difficult physical interpretation include the work of Chang and Dhir [5], who studied the decay in open tubes with tangential inlets but with no contraction. They defined intensity in terms of a *"tangential momentum"* term. In a swirl dryer, the use of Ω is preferred in the benefit of a straight forward interpretation as the axial decay of G_θ. In a confinement with smooth walls, the decay owes to the action of the tangential wall shear stress $\tau_{w,\theta}$ in the velocity field, which is given below from the Reynolds averaged equation of the angular momentum in cylindrical coordinates, for an incompressible, stationary and axi-symmetric vortex [4].

$$\tau_{w,\theta} = \frac{\rho}{R^2} \int_0^R r^2 \frac{\partial}{\partial z}\left(\overline{U}_\theta \overline{U}_z + \overline{u_\theta u_z} - \upsilon \frac{\partial \overline{U}_z}{\partial z}\right) dr \tag{8}$$

Eq. (8) illustrates that the change in the angular momentum flux contained in the convective flow $\overline{U}_\theta \overline{U}_z$ between two sections owes to the moments exerted on the fluid by three shear stresses: that at the wall, and those coming from the turbulent and viscous terms. A very common assumption in pipes consists of considering the wall as the main contributor, and neglect the stresses originated by $\overline{u_\theta u_z}$ and the axial development $\upsilon \partial(\overline{U}_z)/\partial z$. In this way one may describe the rate of change of Ω as the non-dimensional

tangential wall shear stress, combining (7) and (8) to the expression given in (9) for where velocities have been normalized by $\overline{U}_{av}$ and the axial distance z by the cylinder diameter, D.

$$\frac{2\tau_{w,\theta}}{\frac{1}{2}\rho\overline{U}_{av}^2} = \frac{d\Omega}{d(z/D)} \tag{9}$$

$$\Omega = \Omega_{ref} \cdot e^{-\lambda\left(\frac{z-z_{ref}}{D}\right)} \tag{10}$$

The axial variation of Ω shown in (10) provides the background to the experimental evidence of an exponential decay in open pipes. However, Eq. (10) is only a realistic approximation at small values of Ω where $\tau_{w,\theta}$ and Ω are proportional [3] or Steenbergen and Voskamp [4]). According to the measurements of Kitoh [3], strictly speaking this occurs only for $\Omega < 0.04$ in an open pipe. At a higher Ω range the relation between $\tau_{w,\theta}$ and Ω requires either experimental measurement or the estimation from numerical studies (e.g. [44]). The work of Kitoh's (1991) provides data up to $\Omega = 0.9$ and defines the ranges where the piecewise linear relation given in (11) can be assumed to render a slightly more complex decay function in (12), similar to that of Senoo and Nagata [45] where Ω_r and z_r define an initial reference point.

$$\frac{2\tau_{w,\theta}}{\frac{1}{2}\rho\overline{U}_{av}^2} = A \cdot \Omega + B \tag{11}$$

$$\Omega = \left(\Omega_{ref} + \frac{B}{A}\right) \cdot e^{2\cdot A\cdot\left(\frac{z-z_{ref}}{D}\right)} - \frac{B}{A} \tag{12}$$

The study of swirl decay focuses in open pipes where Ω seldom exceeds 1 [4]. Swirl spray dryers operate at far higher values, better represented by the studies of Chang and Dhir [5,6]. They worked at a comparable Ω range to the dryer investigated in this work, and with a similar swirl generation mechanism, in order to promote turbulence and enhance the heat and mass transfer in open tubes. Although carried out at lower Re and in the absence of deposits their results are still useful to compare to the cylindrical chamber of a tall-form dryer. They propose a non-linear dependency to $(z/D)^{0.7}$ and a decay rate strongly correlated to the ratio of the inlet tangential and axial rates, which in a sense remains a measure of geometry and the initial value of Ω, defined here by Ω_i. This correlation was later modified by Erdal [46] or Gomez et al. [47] to include the effect of Re and the number of tangential injectors.

The decay rate, λ or A, is known to be a function of Ω in open pipes and it is expected to decrease for higher Re in a similar manner that the friction factor in fully developed pipe flow. Steenbergen and Voskamp [4] summarize the data over smooth and rough walls and attribute a considerable scatter to the swirl generation mechanisms and the Ω range. Few data are available for the swirl decay in a more restrictive design. In the cylindrical section of combustors, cyclones or dryers, the confinement has a dominant role and the response of the pressure field to an increase in Ω or Re is conditioned by the design of the exit duct. A purely geometric swirl number, similar to Ω_i, is usually defined in these cases according to the design of the inlets, body and outlets [32]. Finally, the wall roughness merits further comment because deposits occur on the walls of any dryer. Wall friction in cyclones has an important effect in the pressure drop and collection efficiency [48] and makes important to develop appropriate numerical models (e.g. [49,50]). In a counter-current swirl dryer the presence of deposits originates a high roughness. This work focuses in studying "cleaned" walls where the roughness height ε varies between 0 and $0.006D$, which is well above the experiments of Senoo and Nagata [45] who report values between 0.0018 and 0.0025 and most of the work reviewed in Steenbergen and Voskamp [4], who nonetheless shows some data with values as high as 0.015.

4. Results and discussion

This part of the paper discusses the influence of the exit contraction in the flow, Section 4.1.1, the self similarity and asymmetries in Sections 4.1.2 And 4.1.3, and the decay of the swirl in Section 4.1.4. The turbulence field is given in Section 4.2, presenting the development of the turbulent kinetic energy, κ, and normal, $\overline{u_i u_i}$, and Reynolds stresses, $\overline{u_i u_j}$, along with the estimates of eddy viscosities, $\nu_{i,j}$, and periodic flow structures.

4.1. Time averaged velocity field

4.1.1. Flow structure and downstream effects

Figs. 3–6 present the time averaged velocity profile, $\overline{U}$, and its decomposition in vertical, tangential and radial direction, $\overline{U}_z, \overline{U}_\theta$ and $\overline{U}_r$, normalized by the superficial air velocity $\overline{U}_{av}$, and for all Re given in Table 1. It includes the radial profiles at different heights in the cylinder, denoted with z, from figures (a) to (h). The error bars represent the maximum error limits, whilst measurements denoted by crosses represent data with a larger deficit error in the velocity.

The centrifugal inertia shifts the point of maximum velocity, $\overline{U}_{Max}$ in Fig. 3 and maximum tangential velocity, $\overline{U}_{\theta,Max}$ in Fig. 5 toward the wall, $r \sim 0.70R$, at the bottom end of the dryer. As the vortex rises, it converges inwards and $\overline{U}_{Max}$ moves to the centre, increasing from $\overline{U}_{Max} = 3.3\overline{U}_{av}$ to $7\overline{U}_{av}$ at the top. Chang and Dhir [5] describe the flow in an open tube at a comparable Ω, and show that the axial flow reverses down at the centre of the vortex due to the adverse pressure gradient caused by the swirl. The reversal however does not occur in a swirl dryer, where a jet forms at the centre in Fig. 4. The suppression of the recirculation is related to the influence of the top boundary, particularly well known in combustors or swirl injectors [12,51]. With no swirl, a contraction causes the acceleration of the flow in its vicinity and a global increase in pressure upstream. In the presence of swirl, these effects are complicated and the entire flow field is affected. The rise in pressure is transmitted down the chamber as a shock wave, which distortions the recirculation and produces a transition to a jet-like velocity profile [11]. A swirl dryer operates a constant flow rate and exit static pressure (see Fig. 1). Therefore, an increase in pressure in the chamber gives rise to higher pressure gradients and the velocities rise. The radial gradients overcome the centrifugal force and the air flow inwards forming a central jet (see Fig. 4) from which the air exits the unit. Escudier and Keller [12] describe how the velocity rise depends on the vortex swirl number because the radial pressure gradient caused by the centrifugal force opposes the inward flow. The higher Ω is, the larger are the radial gradients required to cause the flow inwards, or in other words, the further down the cylinder the influence of the contraction has to be transmitted. Fig. 4 shows that in this case, the contraction is sufficient to develop a jet across the entire cylinder, which confirms the reports of Sharma [22] or Bayly et al. [28] in tall-form dryers at isothermal conditions and associated simulations (e.g. [23,24]), but in turn contrasts experimental data [29] under actual operation conditions, where the sprays seem to hinder the formation of the jet.

Clearly, a rise or a reduction in Ω would modify the effect of the contraction in the flow structure. Different flow regimes have been correlated to the Ω range that prevails in the chamber [33], but in the case treated here of "cleaned" walls, $\overline{U}_z$ remains positive and shows two maxima: a central jet associated to the diameter of the vortex finder and one nearby the wall, related to the centrifugal inertia. As the flow approaches the top the velocity of the jet increases from 1.1 to $1.4\overline{U}_{av}$ for $z \leqslant 5.7D$ to values $> 5-6\overline{U}_{av}$ close

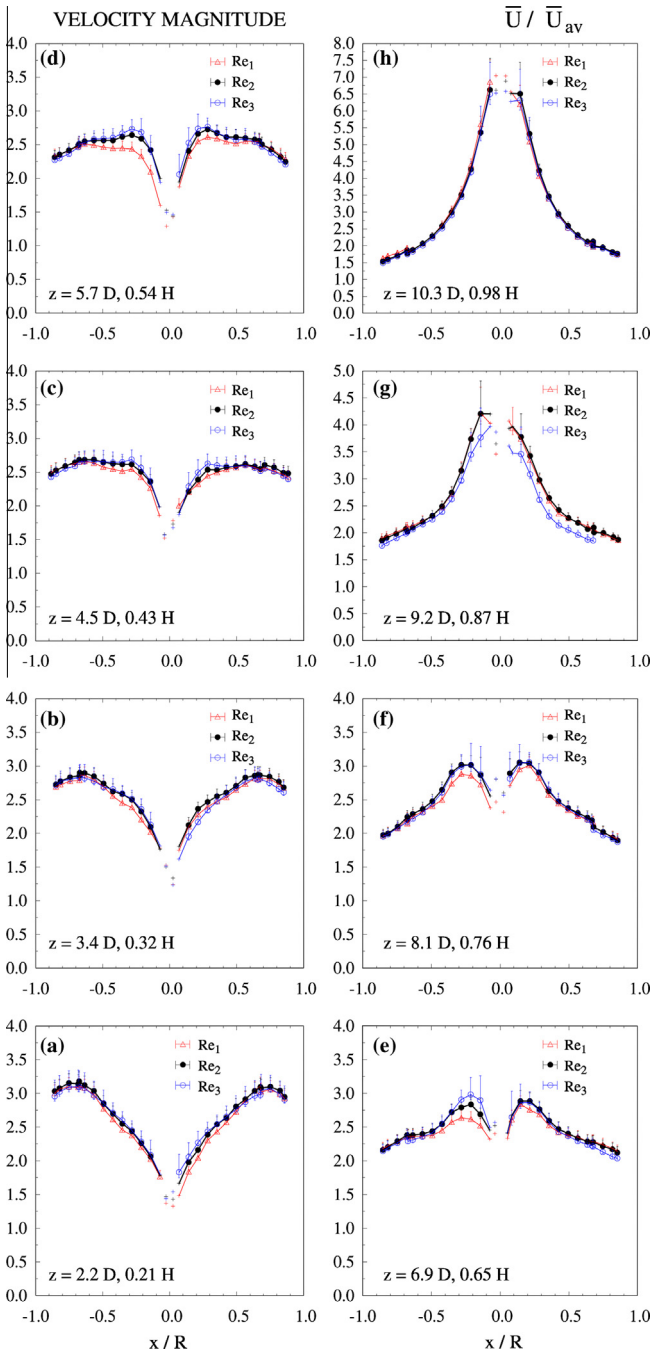

Fig. 3. Velocity magnitude along the cylinder, $\overline{U}(x = -r$ for $\theta < \pi$ and $x = r$ for $\theta < \pi)$.

to the top. In parallel, the axial flow reduces in the outer region. The value of $\overline{U}_{z,Max}$ near the wall drops from 1.5 to $1.8\overline{U}_{av}$ to values $< 1\overline{U}_{av}$ at $z = 10.3D$, where the minimum is lost and the profiles become very similar to the data of Escudier et al. [11] and Derksen [13].

In regards to the swirl, comparison to ideal patterns defined by $\overline{U}_\theta = C \cdot r^n$ aids in the analysis of complex systems [42]. A forced vortex (i.e. solid body rotation) is defined by $n = 1$ while a free-like structure (i.e. potential vortex) shows an inverse relation between $\overline{U}_\theta$ and r defined by $n = -1$, descriptive of irrotational flows such tornados or whirlpools. Comparison to the Burgers solution or Rankine ideal patterns serves to study vortices of the so called *"concentrated"* type, which are comprised of an inner forced vortex and an outer free-like structure. Actual experimental profiles include a transition region nearby the location of $\overline{U}_{\theta,Max}$, where the gradient diminishes and blends both structures. According to these definitions, the flow may be divided into four regions: 1 – an inner forced vortex, 2 – an annular or transition region, 3 – an outer free-like vortex, and 4 – the boundary layer. Fig. 5 shows how the vortex develops a large transition region at the bottom of the tower, between $r \sim 0.10$ and $0.80R$. As the flow rises the location of $\overline{U}_{\theta,Max}$ moves inwards from $r \sim 0.70R$ to $0.20R$ and the transition region narrows substantially, particularly between the levels $z = 3.4D$ and $5.7D$. Above this point, the outer region shows a linear decrease of $\overline{U}_\theta$ with r, between $z = 6.9D$ and $8.1D$, which then develops into an inverse relation at $z = 10.3D$. At this point the transition region is restricted to between $r \sim 0.15R$ and $0.20R$ and the profile follows closely a Rankine pattern. In every level the forced vortex is contained within the jet, and shows a constant radius $r \sim 0.15R$. The transfer of the angular momentum inwards makes $\overline{U}_{\theta,Max}$ to increase axially, and shifts its location to the centre where a forced vortex core of high $\overline{U}_\theta$ appears in $z \geq 5.7D$. In parallel, $\overline{U}_\theta$ decreases in the outer region from $\sim 3.0\overline{U}_{av}$ at $z = 2.2D$, $r = 0.70R$ to values $< 2.0\overline{U}_{av}$ and $1.5\overline{U}_{av}$ moving from $z = 6.9D$ to $10.3D$. The shapes of the profiles agree well with experimental and numerical studies in smaller scales and confirm the observations of Sharma [22]. However, the data show a much larger axial decrease in $\overline{U}_\theta$. Comparison against the data in a scaled down clean tower [28] shows a deficit from 27% to 37% in $\overline{U}_\theta$ at $r = 0.70R$ and levels $z = 0.30H$ and $0.90H$ respectively. This error range confirms past observations in full scale dryers. Hassal [7] reported Particle Image Velocimetry, *PIV*, data near the wall in a full scale and similar operation conditions. The comparison to Bayly et al. [28] showed very similar differences in $\overline{U}_\theta$, from 30% to 40% lower values for the same heights, and $r = 0.91R$. The discrepancies between data in full scale or laboratory dryers owe to a different wall roughness and the effect of friction, discussed in Section 4.1.4.

Radial velocities are given in Fig. 6. Despite a higher uncertainty, certain levels show significantly higher values than expected from continuity in Eq. (2) (see Fig. 6c or e) what suggests the presence of a consistent transversal flow, often neglected in numerical models, and an asymmetrical flow structure discussed in Section 4.1.3.

4.1.2. Self similarity

Comparison across the range of *Re* is included in Figs. 3–6. All the velocities collapse into a characteristic profile when they are normalized by $\overline{U}_{av}$, in agreement with the self-similar nature of swirling flows at a sufficiently large *Re* number (e.g. [52]). An increase in rate and thus $\overline{U}_{av}$ and *Re* simply causes an increase in $\overline{U}$ at any point in the vortex structure, but no changes to its direction. In this way, no differences should be expected in the friction factor (see Section 4.1.4) nor in the effects caused by the contraction. The exception is the behavior of three dimensional asymmetries described below, and the deviations observed for $\overline{U}_\theta$ at the lowest range at Re_1 in Fig. 5d and e.

4.1.3. Asymmetry

The asymmetries in Figs. 3–6 are likely related to the design of the exit and the swirl generation mechanism. The use of tangential inlets is known to develop asymmetric structures (i.e. [53]), which can be avoided by placing a sufficient number of inlets in a symmetrical arrangement. In counter-current dryers, the generation of the vortex is more complex because it does not respond directly to the tangential injection but also to the design of the bottom end of the unit, see Fig. 1a. Huntington [2] lists the usual design in large swirl towers and Sharma [22] or Harvie et al. [23] describe the

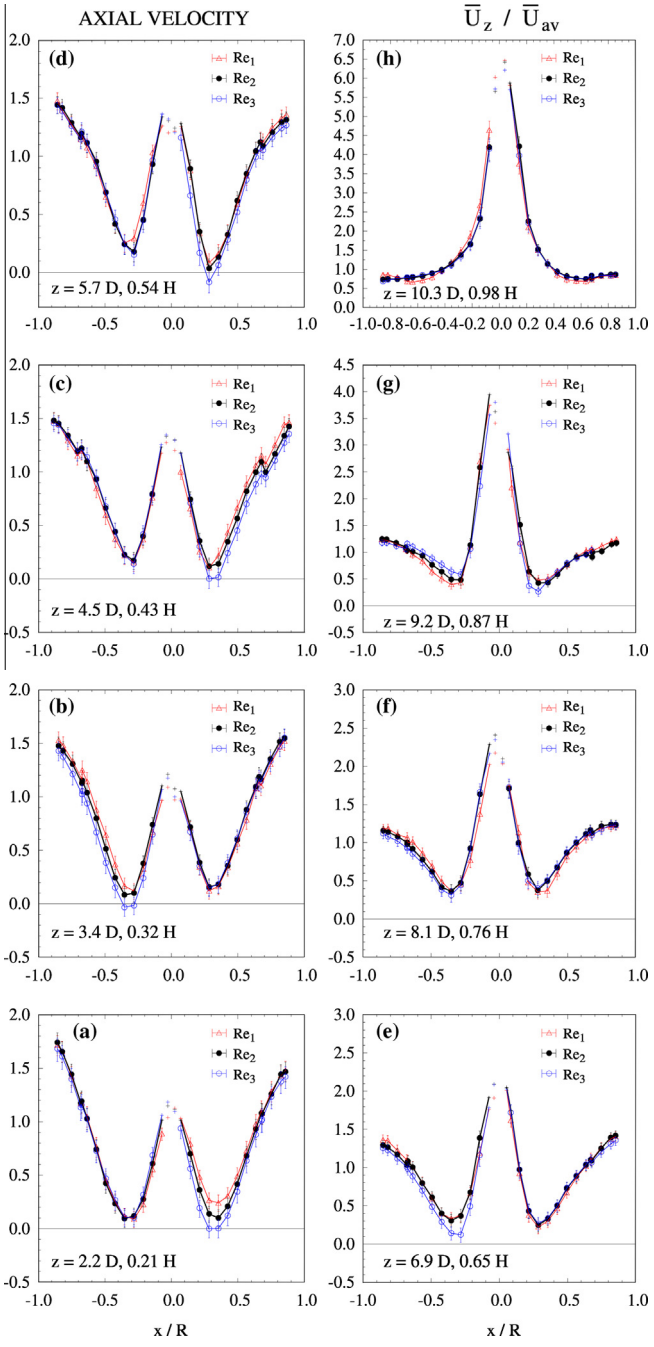

Fig. 4. Axial velocity $\overline{U}_z$ associated to the vortex in Fig. 3.

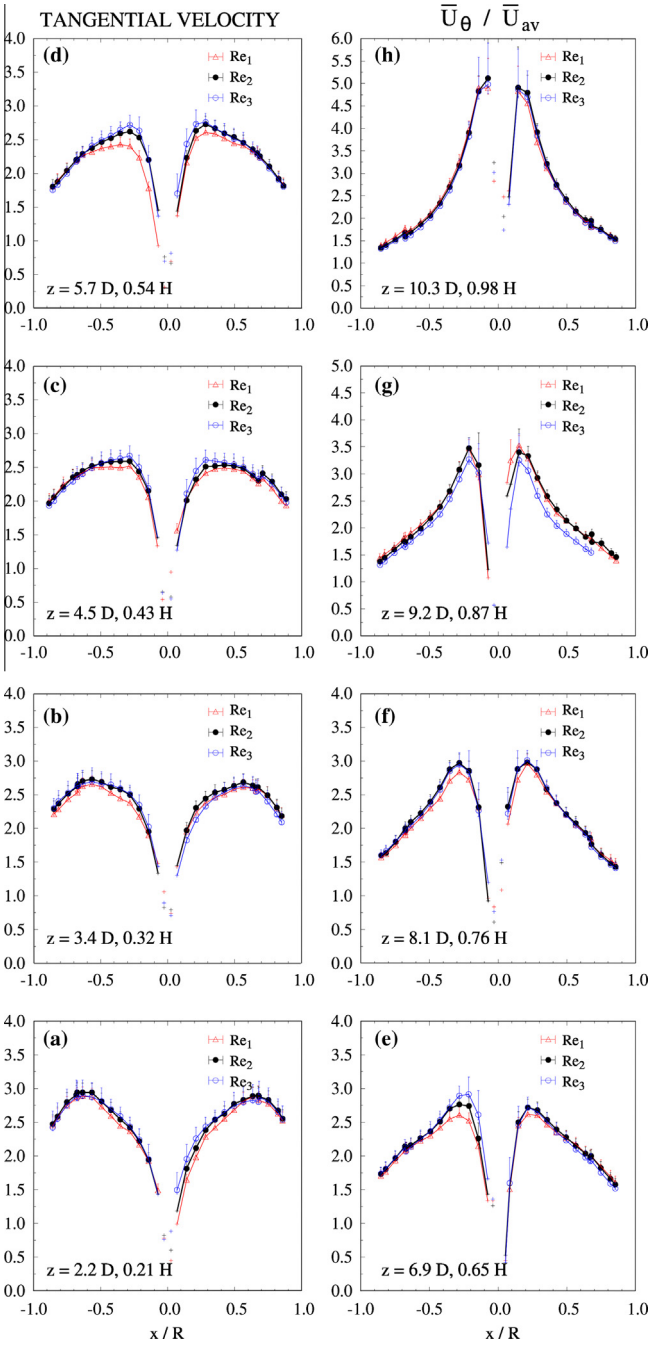

Fig. 5. Tangential velocity $\overline{U}_\theta$ associated to the vortex in Fig. 3.

sensitivity of the vortex shape to the orientation of the inlets. They discuss the difficulties to obtain stable patterns, for which attaining a good balance between the pressures at all inlet ports is fundamental.

Most of data shown are not fully axi-symmetric. Differences are particularly visible in Fig. 4, for the values of $\overline{U}_{z,Max}$ close to the wall and $\overline{U}_{z,Min}$. At the bottom level, $\overline{U}_{z,Max}$ varies from $1.8\overline{U}_{av}$ to $1.5\overline{U}_{av}$ between both sides of the cylinder, while $\overline{U}_{z,Min}$ ranges between $0.1\overline{U}_{av}$ to $0.3\overline{U}_{av}$ for Re_1. As the flow rises, the asymmetry in the outer region stabilizes, but it persists within the transition to the jet. The correlation with *Re* is of interest: whilst one side remains self-similar, the opposite varies significantly. The location where $\overline{U}_z$ varies appears to spiral upwards in the cylinder from $z = 2.2D$ to $6.9D$ (see the tangential position of the accesses in Fig. 1a and its correlation to Fig. 4). Such a pattern points to a coherent asymmetric flow structure, a consequence perhaps of a difference mass rate at some of the inlet ports. As *Re* increases $\overline{U}_{z,Min}$ drops in all these locations, which could be explained by a better equilibration of the flow in the distributor when the pressure drop decreases at higher *Re*. At the top of the unit, asymmetries occur in both $\overline{U}_z$ and $\overline{U}_r$, indicating a strong transversal flow (i.e. from one side to another in the cylinder). At $z = 9.2D$, lower *Re* results in an improved symmetry, which is attributed to the design of the vortex finder. The exit duct includes a series of inner channels that break the swirling motion and often become partially block, forming preferential paths.

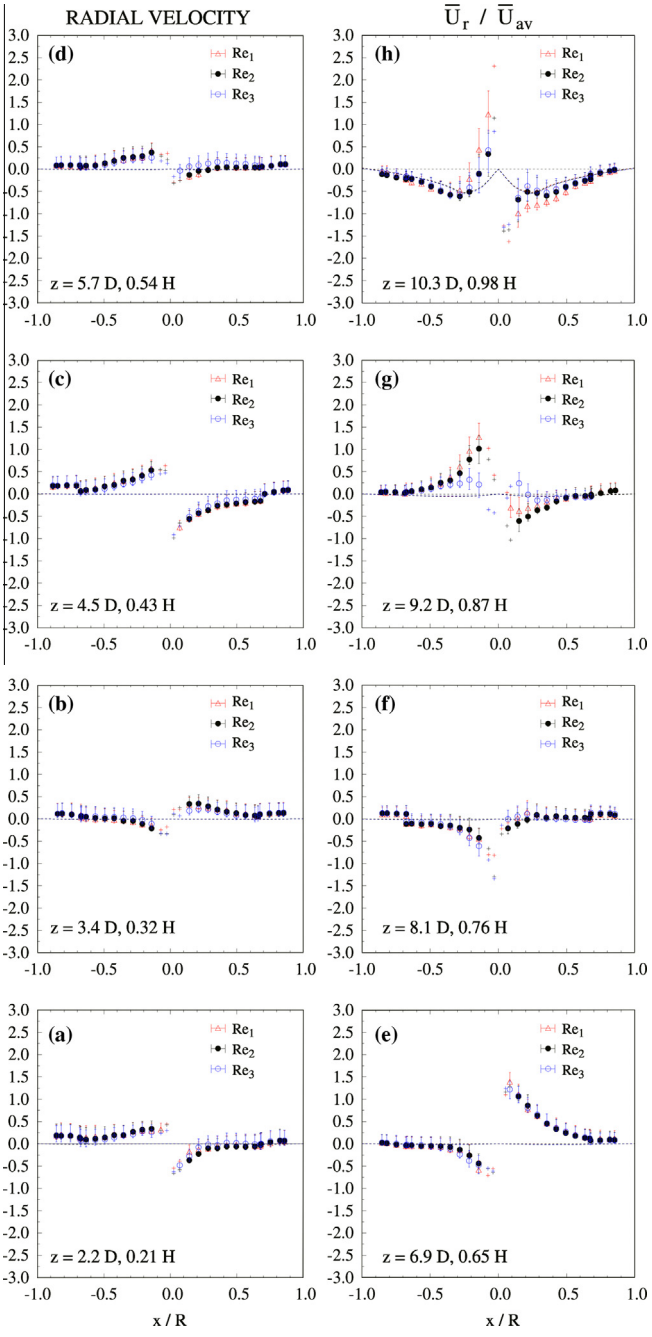

Fig. 6. Radial velocity $\overline{U}_r$ associated to Fig. 3. Lines show the estimation based on (2).

4.1.4. The decay of the swirl

Fig. 7 presents the decay of the swirl intensity Ω along the cylinder. Fig. 7a shows that for such high Ω values the decay does not follow Eq. (10), which suggests the wall shear stress $\tau_{w,\theta}$ is not proportional to Ω. The evolution is better approximated by the piecewise linear relation assumed in Eq. (12). It should be noted that the method does permit measurement of velocities close to the wall. Figs. 4 and 5 show the range extrapolated, and used in Eq. (7) for the calculation of Ω. Three values are given according to the way in which $\overline{U}_z$ and $\overline{U}_\theta$ are reconstructed. The best estimate, Ω_o, is obtained by a linear extrapolation from the last measurement to an intermediate point after which the velocity follows the logarithmic law of the wall. The thickness of this region is set according to the condition of the volume rate complying with the integration of $\overline{U}_z$. In order to give perspective on the absolute maximum errors, the following estimates are also computed according to, (a) a linear decrease of the velocity from the last measurement to zero at the wall, which causes under prediction of Ω and the air flow rate, denoted Ω_- (b) a constant value, causing over prediction of both, denoted Ω_+. The data provided by Bayly et al. [28] or Hassal [7] indicate velocities do not start decaying sharply close to the wall up to $r > 0.98R$ for at least $\overline{U}_\theta$. As a result, Ω_- yields far greater errors in the integration of the mass rate. Errors in the mass rate used to compute Ω_o are kept <0.1% in all cases.

The decay rates from the fit to Eqs. (10) and (12) are summarized in Table 2. The decay rate λ in a smooth pipe rises with increasing Ω and decreasing Re [44,54]. A swirl dryer operates at much higher swirl intensity, which explains why the values of λ between 0.08 and 0.09, are significantly above the usual in pipe flow, which range between 0.019 and 0.032 for $5 \cdot 10^4 < Re < 3 \cdot 10^5$ [4] or between 0.02 and 0.06 for $10^4 < Re < 10^5$ in the work of Najafi et al. [44]. The open tube studied by Chang and Dhir [5] provides a comparable case to a swirl dryer but at a lower $Re = 1.2 \cdot 10^4$ and shows that λ ranges between 0.06 and 0.11 for $\Omega_r = 1.6 - 3.9$. However, in the dryer, the decay rates are found comparable despite working at much higher $Re > 10^5$. In fact λ is found independent of Re in the range studied, see Fig. 7b.

Several considerations follow. Firstly, the stronger swirl decay is related to the roughness of the walls caused by a thin layer of particulate deposits. Interestingly, λ is within the same order of magnitude of the friction factor expected for coarse roughness in a fully developed pipe flow, 0.08 or 0.02 for the Darcy and Fanning friction factors at $\varepsilon/D = 0.05$ [55]. This withstands the assertion of Steenbergen and Voskamp [4] who discuss a general relation between λ and the friction factor for smooth open pipes, and whose correlation does not hold here in a rough flow. Secondly, the lack of correlation between λ and Re is also due to a high roughness. The traditional view of pressure drop in a rough pipe states that when the height of the roughness elements ε stands above the extension of the viscous sub-layer, the friction starts to depend exclusively on ε/D. For the range used here, $\varepsilon/D \sim 0.006$, the friction factor in rough pipes becomes independent of Reynolds numbers precisely for $Re > 10^5$ [55]. Finally, the confinement is likely to reduce the sensitivity of λ to Re, because the higher the centrifugal force is the stronger is the influence of the contraction in the velocity profiles. Thus the relation between $\tau_{w,\theta}$ and Ω (i.e. λ) becomes a stronger function of Ω and less sensitive to Re and the development of a boundary layer [54].

The data provide evidence that full scale dryers operate under a high level of friction. One must stress the importance of finding ways to characterize deposits and account for their effect in the fluid dynamics. The implications for numerical modeling should not be ignored. Large scale computational fluid dynamics, *CFD*, models using smooth wall assumptions over-predict $\overline{U}_\theta$ at the top of the tower by 30–40%. The use of wall functions in a swirling system remains a challenging task [56], and inclusion of these effects entail operating out of the limits of the standard functions for an unidirectional flow in rough walls (e.g. [9]). In these circumstances, it is unclear how boundary conditions may be treated if roughness elements in the order of *mm* or *cm* govern the friction. Perhaps more importantly, it is unclear which impact friction brings to the generation of turbulence and the structure of the boundary layer, both fundamental aspects in particle flow and wall deposition. The reason for friction having remained unnoticed lies in the challenge of obtaining full scale data [2,29]. Numerical works rarely benefit from data in production units but gain validation from laboratory or pilot-scale facilities that serve as valid guides for design purposes but cannot easily replicate the

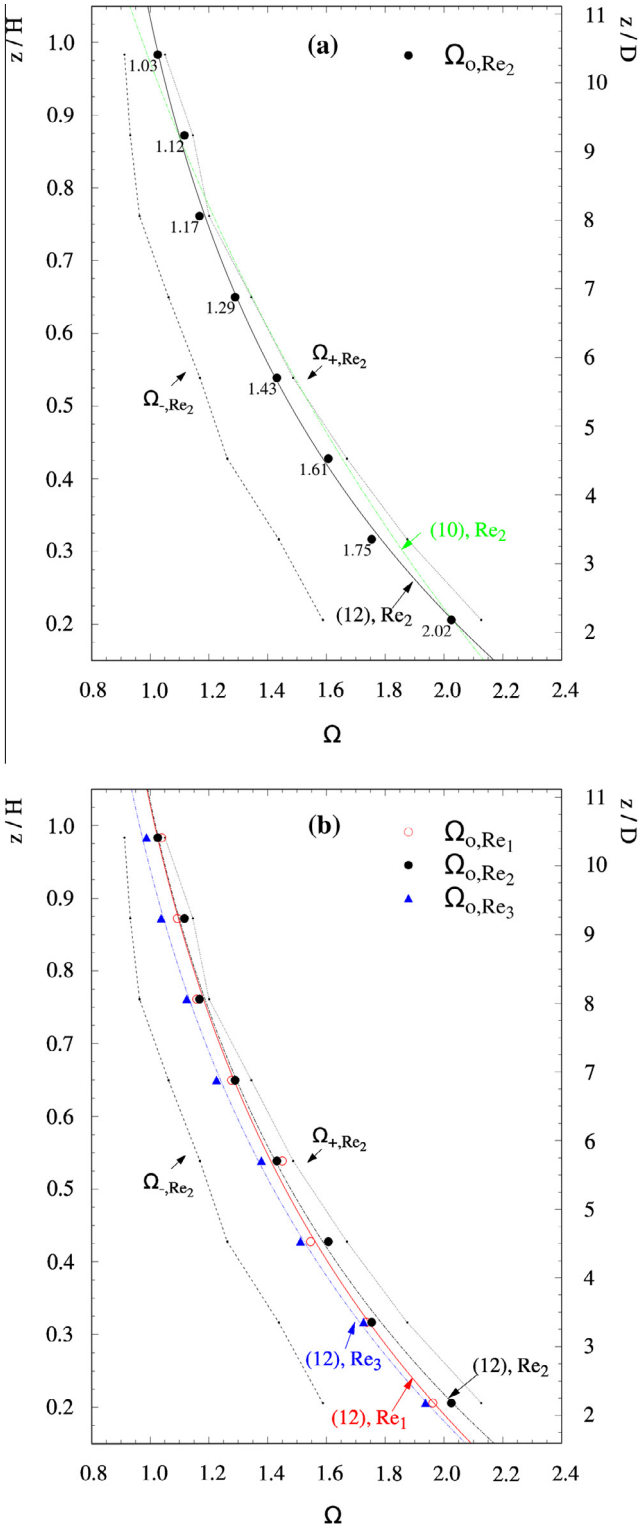

Fig. 7. Axial decay of Ω across the cylindrical chamber. Ω_o, Ω_+ and Ω_- provide respectively the best estimate and over and under predictions of Ω. (a) Fit to Eqs. (10) and (12). (b) Effect of *Re*.

Table 2
Swirl decay rates. Fit to a proportional or linear relation between $\tau_{w,\theta}$ and Ω in (10) and (12).

Case	Ω_{ref}	A	B	λ
Re_1	1.96	−0.080	0.054	0.085
Re_2	2.02	−0.086	0.061	0.089
Re_3	1.93	−0.081	0.051	0.090

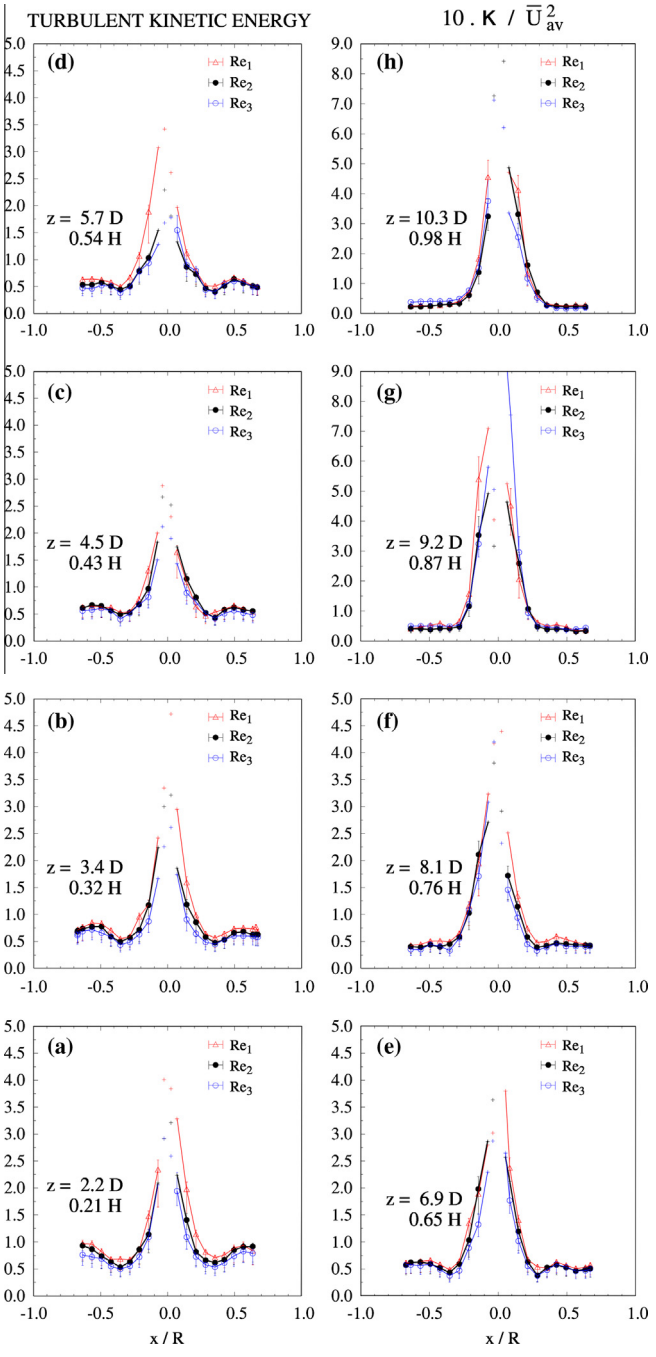

Fig. 8. Turbulent kinetic energy, κ, associated to Fig. 3 at all values of *Re* in Table 1.

characteristics of production. Having ignored the friction has potentially caused fully coupled models to contain severe bias errors in the prediction of particle centrifugal inertia, known to be critical in swirl units where the interaction with the wall is fundamental [8].

4.2. Turbulence statistics and periodicity

4.2.1. Turbulent kinetic energy and intensity

The turbulent kinetic energy, κ, is reported in Fig. 8 for all positions and *Re*. Figs. 9 and 10 present the decomposition in

normal stresses for the outer region. A large maximum in κ is observed in every level at the centre of the tower, varying from 0.2 to $0.3\overline{U}_{av}^2$ at the bottom to $> 0.7\overline{U}_{av}^2$ at 9.2*D* and down to $0.3–0.5\overline{U}_{av}^2$ at the top. The region of high variability agrees well with the extension of maximum in the axial velocity, and is likely to be the result of an unstable jet, commonly reported in cyclonic flows (e.g. [57,58,53]).

Vortices present aerodynamic instabilities when the strength of the swirl increases. For low *Re*, local recirculation starts for swirl numbers >0.6 in a straight exit type of device. The stagnation of the flow [15] leads to various types of *VBD* depending on the flow characteristics and the geometry of the system, which is subject of ample research in aeronautics or combustion [59]. For sufficiently large *Re* the instability manifests by formation of periodical structures. The breakdown then results in a coherent oscillation whereby the core of the vortex precesses around its symmetry axis, referred to as the *PVC* and widely reported in combustors [14], the exit duct of cyclones [15,16,48] and the inlet of co-current dryers [21]. The conditions for its occurrence, its characteristics and its transmission are highly dependent on *Re*, *Ω*, the confinement, and the condition of the flow between the *CRZ*, the *VBD* and the exit, i.e. subcritical of supercritical according to its ability to withstand or not inertial waves [12].

Put simply, the *PVC* responds to the instability of the core causing it to acquire a spiral shape around which axis fluctuates in a helical orbit. It becomes identifiable by its effect on velocity variability. The velocity variance at a fixed point in the region affected by *PVC* comprises of a turbulent term and a periodic signal owed to the fluctuation of the relative position between the observer and the core. This sort of phenomenon is responsible for the large central maximum observed in Fig. 8 associated with no turbulent energy but indicative of the unstable nature of the core, see Section 4.2.4.

Fig. 9a presents the radial and axial development of κ. The outer region shows comparable values and profiles to the data in an open

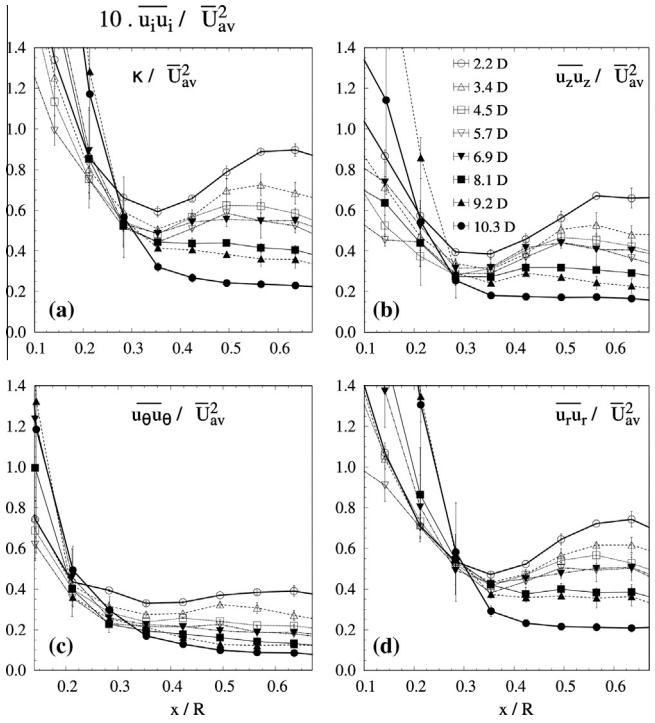

Fig. 9. Axial variation of normal stresses at Re_2 in Table 1. (a) κ, (b) $\overline{u_z u_z}$, (c) $\overline{u_\theta u_\theta}$, and (d) $\overline{u_r u_r}$. Error bars indicate the variation across tangential locations. The maximum uncertainty ranges are −31%, +7% for κ, −41%, +19% for $\overline{u_z u_z}$, −23%, +19% for $\overline{u_\theta u_\theta}$, and −35%, +22% for $\overline{u_r u_r}$ [38,39].

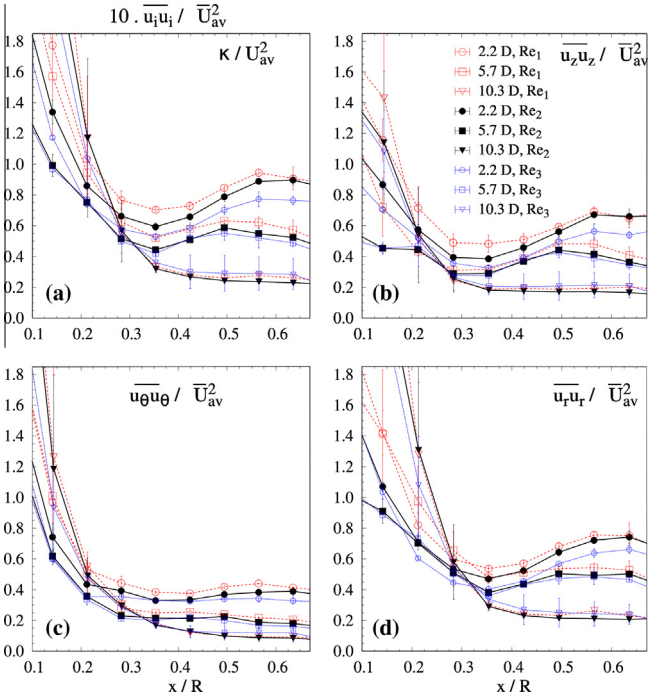

Fig. 10. Impact of *Re* upon the normal stresses. (a) κ (b), $\overline{u_z u_z}$, (c) $\overline{u_\theta u_\theta}$, and (d) $\overline{u_r u_r}$. Error bars indicate the variation across tangential locations. The maximum uncertainty ranges are given in Fig. 9.

tube [5]. The maximum outer value κ_{Max} moves inwards as the flow approaches the exit, and κ decrease axially from between 0.06 and $0.09\overline{U}_{av}^2$ to $0.02–0.03\overline{U}_{av}^2$, following a linear relation to the decay of Ω suggested by Chang and Dhir [5]. The normal stresses $\overline{u_z u_z}$ and $\overline{u_r u_r}$ show the same transition between the inner jet and outer regions, ranging between 0.02 and $0.07\overline{U}_{av}^2$ at the bottom, to $0.02–0.03U_{av}^2$ close to the exit (see Fig. 9b and d). Both present an outer maximum that converges inwards with increasing height. The turbulent mixing in the azimuthal direction is given by $\overline{u_\theta u_\theta}$ (Fig. 9c). In contrast to an open tube where all normal stresses are similar, $\overline{u_\theta u_\theta}$ is 30–40% lower than $\overline{u_r u_r}$ and $\overline{u_z u_z}$ and shows no outer maximum. Such behavior can be explained by the effect the contraction according to Large Eddy Simulations, *LES*. Derksen [13] described the disruption caused upstream by an exit contraction, and showed the evolution of the vortex structure in tubes moving from an open system to high contraction ratios. An open cylinder shows an inner stabilizing forced vortex and a highly turbulent outer free vortex. Moving into narrow contractions, the core is distorted and Taylor–Görtler vortices appear in the outer region, suppressing mixing in the azimuthal direction. Finally, Fig. 10 shows that κ and normal stresses are reduced with increasing *Re*, particularly at the bottom of the unit where the differences are significant.

4.2.2. Reynolds stresses

Figs. 11 and 12 present the development of Reynolds stresses. $\overline{u_z u_\theta}$ is associated to the transfer of angular momentum downstream due to the turbulence, and thus is predominantly positive (see Fig. 11a). It shows a maximum at $r = 0.58R$ that moves inwards when the angular momentum flux is transferred to the jet. $\overline{u_z u_\theta}$ decays axially, in agreement with the decay of Ω and the behavior observed in open tubes [5]. In contrast, two zones of negative values appear in this case: 1 – at the inner region also noticed in by Chang and Dhir [5], who in general report higher values and 2 – at the vicinity of the top exit, $z = 10.3D$, indicative of the recirculation originated at the dead regions above.

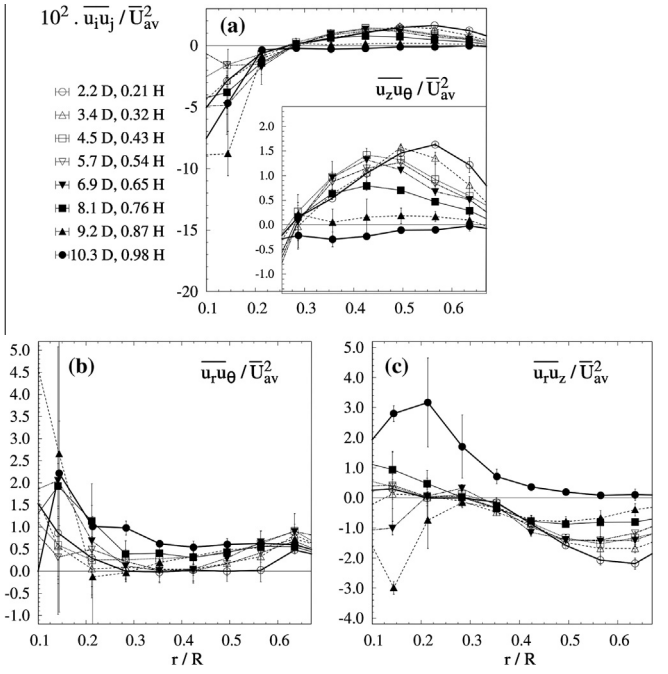

Fig. 11. Development of the Reynolds stresses at Re_2 in Table 1). (a) $\overline{u_z u_\theta}$, (b) $\overline{u_r u_\theta}$, and (c) $\overline{u_r u_z}$. Error bars indicate the variation across tangential locations. Maximum uncertainty ranges are for $\overline{u_z u_\theta}$, ±60%, for $\overline{u_r u_\theta}$ ± 100% and for $\overline{u_r u_z}$, ±200–400% [38,39].

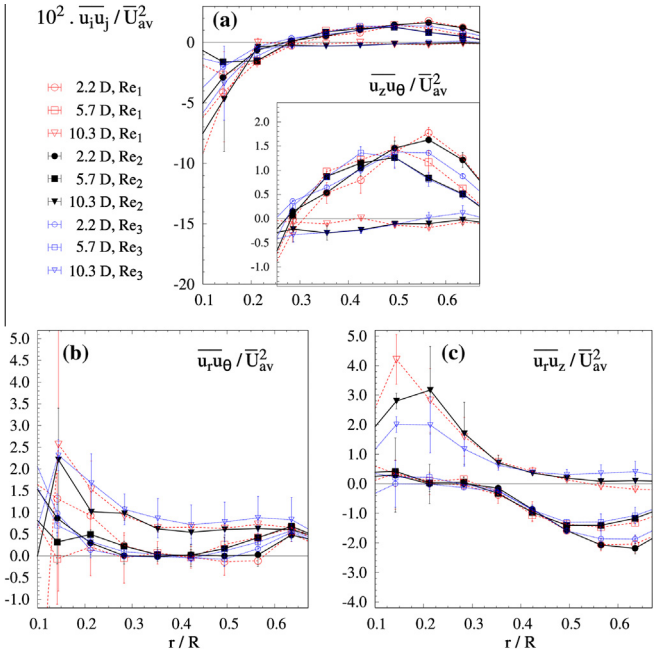

Fig. 12. Impact of *Re* in the development of Reynolds stresses. (a) $\overline{u_z u_\theta}$, (b) $\overline{u_r u_\theta}$, and (c) $\overline{u_r u_z}$. Error bars indicate the variation across tangential locations. The maximum uncertainty ranges are given in Fig. 11.

$\overline{u_r u_\theta}$ increases axially in Fig. 12b showing positive values and a similar transition at the jet between $r = 0.25$ and $0.30R$, where it is predominantly positive. $\overline{u_r u_z}$ takes large negative values in the outer region and shows a similar range and evolution to an open tube [5]. The values drop axially, and acquire a positive sense only close to the exit. A similar transition occurs at the inner region, where $\overline{u_r u_z}$ change direction between $z = 6.9D$ and $10.3D$. In contrast to the behavior of normal stresses, no changes can be

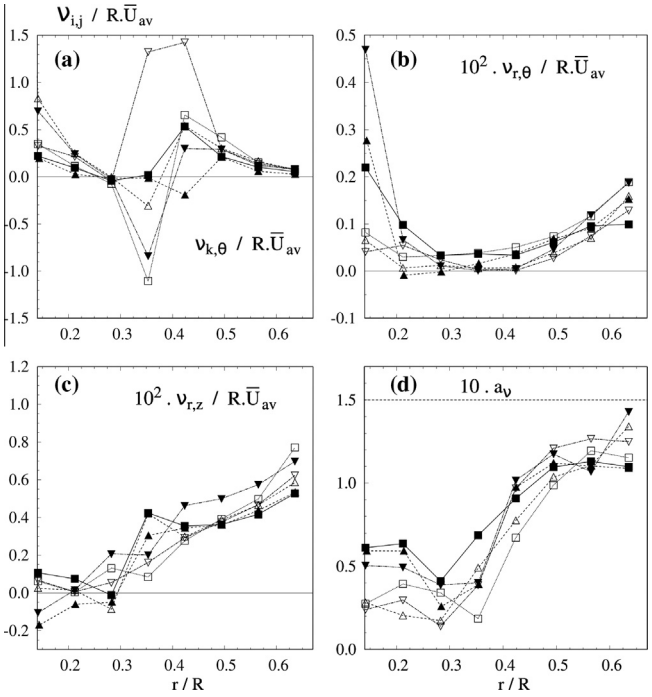

Fig. 13. Anisotropy, and eddy viscosities for all levels at Re_2 in Table 1. For nomenclature see Fig. 11. (a) $\upsilon_{z,\theta}$, (b) $\upsilon_{r,\theta}$, (c) $\upsilon_{r,z}$ and (d) $a_\upsilon = (\overline{u_r u_z}^2 + \overline{u_r u_\theta}^2)/2\kappa$.

observed in the development of the Reynolds stresses as a function of *Re* in Fig. 12.

4.2.3. Eddy viscosity and anisotropy

Eddy viscosities are summarized in Fig. 13. $\nu_{z,\theta}$ shows a transition at $0.35R < r < 0.40R$ where $\partial\overline{U}_\theta/\partial z$ achieves its locus (see Fig. 13a), thus defining the regions where the axial change of $\overline{U}_\theta$ is dominated by wall friction (i.e. at a higher r) or by the transfer of angular momentum inwards caused by the influence of the exit (i.e. at a lower r). In the transition region $\nu_{r,\theta}$ shows a minimum and maintains positive values, but $\nu_{r,z}$ decreases from large positive in the outer region to low values at the centre where it can turn negative (indicative of negative turbulence energy production).

Comparison of the of $\nu_{z,\theta}$ to $\nu_{r,\theta}$ and $\nu_{r,z}$, show a substantial difference, in the same order of magnitude than the reports of Kitoh [3] and Chang and Dhir [5]. The data confirm the ample evidence of the mixing length theory not being able to describe anisotropy in swirling flows. An anisotropy factor a_f has been estimated as the ratio of the shear stress to $2\cdot\kappa$ in the same manner as Kitoh [3]. a_υ varies significantly in the radial direction, and increases axially. In agreement with the observations in pipe flow a_υ also tends to 0.15 in the outer region and diminishes substantially in the transition inwards, taking values between 0.01 and 0.04. However in this case, a_υ rises again at the jet.

4.2.4. Precession of the vortex core

This work focuses in studying the structure of the flow at large scale. In this context, the use of sonic anemometry is beneficial despite it entails working with lower accuracy than laser-based techniques. Having said that analysis of the time scales contained in the velocity signal produce reasonable results and reveals periodicity at various time scales. High-amplitude oscillations and long history effects are a common feature of the inner vortex of cyclones or in co-current spray dryers. Fig. 14a presents an example of the same behavior in a counter-current unit by showing the velocity signal at several positions. At the top section of the vortex core,

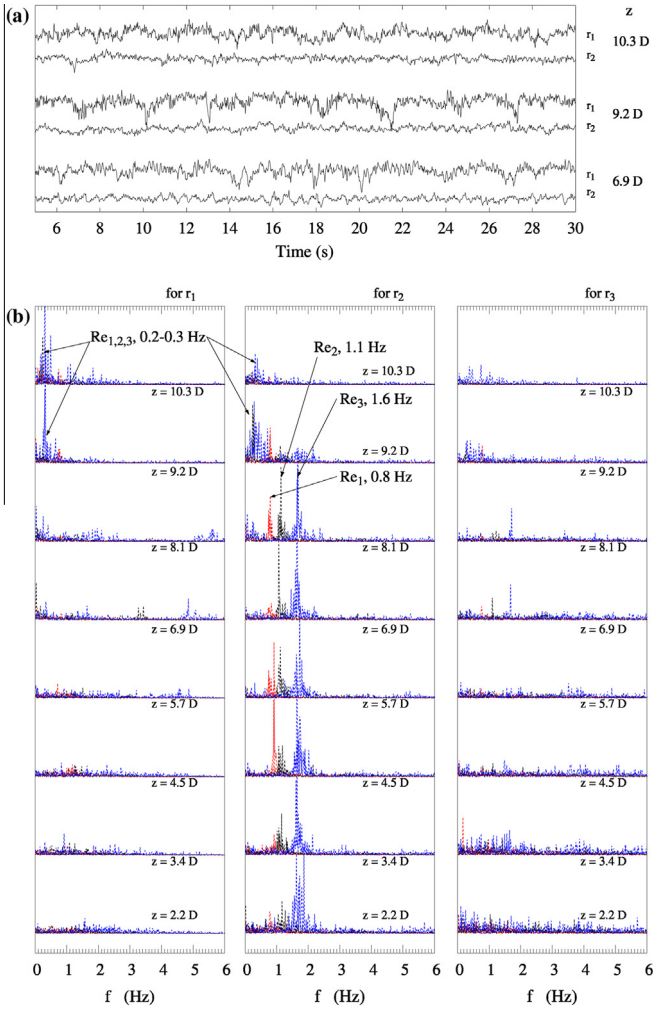

Fig. 14. Periodical flow structures. Analysis at $r_1 = 0.14R$, $r_2 = 0.35R$, $r_3 = 0.57R$. (a) Times series for U_θ. (b) Periodogram of U for all heights at the inner region r_1 (left), transition r_2 (centre) and outer region r_3 (right). Arbitrary y unit; scaling changes from 1 on r_2 or r_3 to 0.5 on r_1.

an oscillation in the order of seconds is superimposed upon faster fluctuations owed to the turbulence. Fig. 14b analyses the different time scales with a *FFT*. The correlation of periodicity, position and *Re* is illustrated by superimposing the periodograms obtained for *U* at the inner and outer vortices, and the transition between both. Several periodic signals are visible, (a) a large time scale oscillation appears in the core, restricted to the top of the dryer, $9.2D \leq z \leq 10.3D$, and (b) an oscillation at a higher frequency occurs in transition to the inner vortex, between $r = 0.20R$ and $0.35R$ and extends upstream in the cylinder from $z = 9.2D$ to levels $< 5.7D$, $3.4D$ or $2.2D$ according to the increase in *Re*.

Periodical structures such as the *PVC* are often characterized by the Strouhal number, *St* ($St = f \cdot D/\overline{U}_{av}$ where f is the oscillation frequency). At large *Re*, the *PVC* in confined units maintains at constant *St* [14], which means that when increasing the bulk velocity in cyclones [15] or [16]) or tangential swirlers [52] the fluctuation occurs faster. Fig. 14b shows the same behavior in a swirl dryer. The oscillation frequency, f, in the transition region increases linearly with the $\overline{U}_{av}$ (from 0.8 to 1.1 and 1.6 Hz for Re_1, Re_2 and Re_3) what means it occurs at a constant $St \approx 1.4$–1.5. In this case no similar correlation with *Re* can be appreciated at top core, perhaps due to the low resolution. The presence of this sort of oscillations at a constant *St* suggests that swirl dryers present a similar preceding core to cyclones where the entire inner jet adopts a sort of helical movement [48]. At some point before or within the exit, perhaps between levels $5.7D \leq z \leq 6.9D$, the high centrifugal force in the forced vortex destabilizes the jet and originates the fluctuation.

5. Conclusions

The swirling air fluid dynamics in a full industrial scale tall-form spray dryer operating at isothermal conditions and in the absence of the solid phase has been described, identifying the following main features:

- A significant role of the confinement and the downstream effects in the vortex structure.
- Consistent field asymmetries.
- The development of a self-similar vortex structure, invariant within the *Re* operating range.
- Strong swirl decay owing to the confinement and presence of particulate deposits at the walls.
- The characteristic turbulence structure, including its anisotropy through the description of normal stresses, and rough estimates of Reynolds stresses and the eddy viscosity ranges
- Periodical structures that oscillate at constant *St*, likely related to the precession of the vortex core.

The phenomena described in this paper, such as the suppression of the recirculation owed to the vortex finder, the mixing owing to the *PVC*, or most importantly the role that friction at the walls has in the swirl decay, were observed in a relevant range of *Re* for a production swirl dryer, and thus will be relevant in isothermal and non-isothermal operation. Of course, one must expect the flow structure to be affected by the density gradients when the solids are present, in addition to the exchange of momentum with the spray which hinders the formation of the jet and the concentration near the wall, which is likely to cause a further attenuation of the swirl. However, fully coupled large scale models currently lack validation and the observations in this work indicate they need to be revised on a fluid dynamics level.

The importance of friction and how this affects the vortex structure needs to be addressed in computational fluid dynamic simulations. Consider that the omission of the swirl decay is responsible of an over prediction of $\overline{U}_\theta > 30$—40% in isothermal models using smooth walls as a boundary conditions. Such an error gains relevance in the prediction of particle dispersion, drying and aggregation because in any tower, the particle dynamics is intimately related with the centrifugal inertia that the solids gain from the air. In essence, the swirl establishes the concentration of particles near the wall and the rates of deposition and erosion, crucial to the process [8]. In addition, description of turbulence and recirculation affect particle residence time and the elutriation of powder. Clearly one must first be able to understand and replicate numerically the air flow structure, stability and swirl decay observed at isothermal cases and in the absence of solids before one can rely in more complex tools. In this line, the study of semi-empirical wall functions for rough walls over pipes and how to apply a similar approach to strong swirling flows must become an area of focus.

Acknowledgments

VF was supported by an Engineering Doctorate Studentship sponsored by the Engineering and Physical Sciences Research Council (EPSRC) and Procter & Gamble in the Industrial Doctoral Centre in Formulation Engineering, School of Chemical Engineering, University of Birmingham.

References

[1] P.W. Appel, Modern methods of detergent manufacture, J. Surfactants Detergents 3 (2000) 3.
[2] D.H. Huntington, The influence of the spray drying process on product properties, Drying Technol. 22 (6) (2004) 1261–1287.
[3] O. Kitoh, Experimental study of turbulent swirling flow in a straight pipe, J. Fluid Mech. 225 (1991) 445–479.
[4] W. Steenbergen, J. Voskamp, The rate of decay of swirl in turbulent pipe flow, Flow Meas. Instrum. 9 (1998) 67–78.
[5] F. Chang, V.K. Dhir, Turbulent flow field in tangentially injected swirl flows in tubes, Int. J. Heat Fluid Flow 15 (5) (1994) 346–356.
[6] F. Chang, V.K. Dhir, Mechanisms of heat transfer enhancement and sloe decay of swirl in tubes using tangential injection, Int. J. Heat Fluid Flow 16 (2) (1995) 78–87.
[7] G. Hassal, Wall build up in spray driers, EngD thesis. University of Birmingham, Birmingham, UK, 2011
[8] V. Francia, L. Martin, A.E. Bayly, M.J.H. Simmons, The role of wall deposition and re-entrainment in swirl spray dryers, AICHE J. (2015), http://dx.doi.org/10.1002/aic.14767.
[9] J. Jimenez, Turbulent flow over rough walls, Ann. Rev. Fluid Mech. 36 (2004) 173–196.
[10] R.J. Volino, M.P. Schultz, K.A. Flack, Turbulence structure in rough- and smooth-wall boundary layers, J. Fluid Mech. 592 (2007) 263–293.
[11] M.P. Escudier, J. Bornstein, N. Zehnder, Observations and LDA measurements of confined turbulent vortex flow, J. Fluid Mech. 98 (1) (1980) 49–63.
[12] M.P. Escudier, J.J. Keller, Recirculation in swirling flow: a manifestation of vortex breakdown, AIAA J. 23 (1) (1985) 111–116.
[13] J.J. Derksen, Simulations of confined turbulent vortex flow, Comput. Fluids 34 (2005) 301–318.
[14] N. Syred, A review of oscillation mechanisms and the role of the precessing vortex core (PVC) in swirl combustion systems, Prog. Energy Combust. Sci. 32 (2006) 93–161.
[15] T. O'Doherty, A.J. Griffiths, N. Syred, P.J. Bowen, W. Fick, Experimental analysis of rotating instabilities in swirling and cyclonic flows, Dev. Chem. Eng. Miner. Process 7 (3/4) (1999) 245–267.
[16] J.J. Derksen, H.E.A. Van den Akker, Simulation of vortex core precession in a reverse-flow cyclone, AIChE J. 46 (7) (2000) 1317–1331.
[17] H. Usui, Y. Sano, Y. Yanagimoto, Y. Yamasaki, Turbulent flow in a spray drying chamber, J. Chem. Eng. Jpn. 18 (1985) 3.
[18] T.A.G. Langrish, D.E. Oakely, R.B. Keey, R.E. Bahu, C.A. Hutchinson, Time dependent flow patterns in spray driers, Trans. IChemE 71 (A) (1993).
[19] F.G. Kieviet, J. Van Raaij, P.P.E.A. De Moor, P.J.A.M. Kerkhof, Measurement and modelling of the air flow pattern in a pilot-plant spray dryer, Trans. IChemE 75 (A) (1997).
[20] D.B. Southwell, T.A.G. Langrish, The effect of the swirl on the stability of spray dryers, Trans. IChemE 79 (A) (2001).
[21] T.A.G. Langrish, J. Williams, D.F. Fletcher, Simulation of the effects of the inlet swirl on gas flow patterns in a pilot-scale spray drier, Chem. Eng. Res. Des. 82 (A7) (2004) 821–833.
[22] S. Sharma, Spray dryer simulation and air flow pattern studies, Ph.D thesis. The University of Aston, Birmingham, UK, 1990.
[23] D.J.E. Harvie, T.A.G. Langrish, D.F. Fletcher, Numerical simulations of the gas flow patterns within a tall form spray dryer, Trans. IChemE 79 (2001) 235–248.
[24] M. Ali, Numerical modelling of a counter-current spray drying tower, PhD thesis. University of Leeds. Leeds, UK, 2014
[25] G. Place, K. Ridgway, P.V. Danckwerts, Investigation of air-flow in a spray-drier by tracer and model techniques, Trans. IChemE 37 (1959) 269–276.
[26] J.R. Paris, P.N. Ross, S.P. Dastur, R.L. Morris, Modeling of the air flow pattern in a counter current spray-drying tower, Ind. Eng. Chem. Process Des. Develop. 10 (1971) 2.
[27] R.B. Keey, Q.T. Pham, Residence time distribution in a tall-form spray chamber, Chem. Eng. Sci. 32 (1976) 1219–1226.
[28] A.E. Bayly, P. Jukes, M. Groombridge, C. McNally, Airflow patterns in a counter-current spray drying tower – simulation and measurement, Int. Drying Symp. (2004) 775–781.
[29] I. Zbicinski, M. Piatkowski, Continuous and discrete phase behavior in countercurrent spray drying, Drying Technol. 27 (12) (2009) 1353–1362.
[30] G. Fieg, G. Wozny, K. Buick, L. Jeromin, Estimation of the drying rate and moisture profiles in an industrial spray dryer by means of experimental investigations and a simulation study, Chem. Eng. Technol. 17 (1994) 235–241.
[31] P. Wawrzyniak, M. Podyma, I. Zbicinski, Z. Bartczak, J. Rabaeva, Modeling of air flow in an industrial counter-current spray drying tower, Drying Technol. 30 (2012) 217–224.
[32] A.K. Gupta, D.G. Lilley, N. Syred, Swirl Flows, Abacus Press, Tunbridge Wills, UK, 1984.
[33] V. Francia, L. Martin, A.E. Bayly, M.J.H. Simmons, Influence of wall friction on flow regimes and scale up of swirl spray dryers, 2015b (submitted for publication).
[34] Gill Instruments Ltd. HS-50, Horizontally symmetrical ultrasonic research anemometer. User manual. no 1199-PS-0032, Issue 02, 2004.
[35] S. Franchini, A. Sanchez-Andres, A. Cuerva, Effect of the pulse trajectory on ultrasonic fluid velocity measurement, Exp. Fluids 43 (2007) 969–978.
[36] A. Cuerva, A. Sanchez-Andres, On sonic anemometer measurement theory, J. Wind Eng. Ind. Aerodyn. 88 (2000) 25–55.
[37] T. Nakai, K. Shimoyama, Ultrasonic anemometer angle of attack errors under turbulent conditions, Agric. For. Meteorol. 162–163 (2011) 14–26.
[38] V. Francia, Spray drying of detergents in counter-current towers; A study of turbulent swirling flows, fouling and agglomeration, EngD thesis. University of Birmingham, Birmingham, UK, 2015
[39] V. Francia, L. Martin, A.E. Bayly, M.J.H. Simmons, Use of sonic anemometry for the study of confined swirling flows in large industrial units, 2015c (submitted for publication).
[40] A. Gil, C. Cortes, L.M. Romeo, J. Velilla, Gas-particle flow inside cyclone diplegs with pneumatic extraction, Powder Technol. 128 (2002) 78–91.
[41] R. Weber, J. Dugué, Combustion accelerated swirling flows in high confinements, Prog. Energy Combust. Sci. 18 (1992) 349–367.
[42] D.G. Sloan, P.J. Smisth, L.D. Smooth, Modeling of swirl in turbulent flow systems, Prog. Energy Combust. Sci. 12 (1986) 163–250.
[43] K.S. Yajnik, V. Aubbaiah, Experiments on swirling turbulent flows. Part 1. Similarity in swirling flows, J. Fluid Mech. 60 (1973) 665–687.
[44] A.F. Najafi, S.M. Mousavian, K. Amini, Numerical investigations on swirl intensity decay rate for turbulent swirling flow in a fixed pipe, Int. J. Mech. Sci. 53 (2011) 801–811.
[45] Y. Senoo, T. Nagata, Swirl flow in long pipes with different roughness, Bullet. JSME 5 (90) (1972) 1514.
[46] F. Erdal, Local measurements and computational fluid dynamics simulations in a gas–liquid cylindrical cyclone separator, Ph.D. thesis, The University of Tulsa, USA, 2001.
[47] L. Gomez, R. Mohan, O. Shoham, Swirling gas–liquid two-phase flow. experiment and modeling Part II: Turbulent quantities and core stability, J. Fluids Eng. 126 (2004) 943–959.
[48] C. Cortes, A. Gil, Modeling the gas and particle flow inside cyclone separators, Prog. Energy Combust. Sci. 33 (2007) 409–452.
[49] C.H. Kim, J.W. Lee, A new collection efficiency model for small cyclones considering the boundary-layer effect, Aerosol Sci. 32 (2001) 251–269.
[50] F. Kaya, I. Karagoz, A. Avci, Effects of surface roughness on the performance of tangential inlet cyclone separators, Aerosol Sci. Technol. 45 (2011) 988–995.
[51] Y.C. Chao, J.H. Leu, Y.E. Hung, C.K. Lin, Downstream boundary effects on the spectral characteristics of a swirling flow field, Exp. Fluids 10 (1991) 341–348.
[52] I.V. Litvinov, S.I. Shtork, P.A. Kuibin, S.V. Alekseenko, K. Hanjalic, Experimental study and analytical reconstruction of precessing vortex in a tangential swirler, Int. J. Heat Fluid Flow 42 (2013) 251–264.
[53] R. Hreiz, C. Gentric, N. Midoux, Numerical investigation of swirling flow in cylindrical cyclones, Chem. Eng. Res. Des. 89 (2011) 2521–2539.
[54] R. Maddahian, A. Kebriaee, B. Farhanieh, B. Firoozabadi, Analytical investigation of boundary layer growth and swirl intensity decay rate in a pipe, Arch. Appl. Mech. 81 (2011) 489–501.
[55] L.F. Moody, Friction factors for pipe flow, Trans. ASME 66 (8) (1944) 671–684.
[56] S. Jakirlic, K. Hanjalic, C. Tropea, Modelling rotating and swirling turbulent flows: a perpetual challenge, AIAA J. 40 (2002) 1984–1996.
[57] A.J. Hoekstra, J.J. Derksen, H.D.A. Van Den Akker, An experimental and numerical study of turbulent swirling flow in gas cyclones, Chem. Eng. Sci. 54 (1999) 2055–2065.
[58] Z. Liu, J. Jiao, Y. Zheng, Q. Zhang, L. Jia, Investigation of turbulence characteristics in a gas cyclone by stereoscopic PIV, AIChE J. 52 (12) (2006) 4150–4160.
[59] O. Luca-Negro, T. O'Doherty, Vortex breakdown: a review, Prog. Energy Combust. Sci. 27 (2001) 431–481.